J. Opt. A: Pure Appl. Opt. **11** (2009) 034014 (6pp) doi:10.1088/1464-4258/11/3/034014

Label-free analysis of microfluidic mixing processes by dynamic phase contrast microscopy

Frank Holtmann, Mathias Eversloh and Cornelia Denz

Institut für Angewandte Physik, Westfälische Wilhelms-Universität, Corrensstrasse 2, D-48149 Münster, Germany

E-mail: frank.holtmann@uni-muenster.de

Received 30 July 2008, accepted for publication 16 October 2008
Published 20 January 2009
Online at stacks.iop.org/JOptA/11/034014

Abstract
We demonstrate a dynamic phase contrast microscope based on photorefractive holographic interferometry. This system allows us to quantify concentration changes during micro-mixing processes by measuring the change of the optical path length. Therefore, no labelling processes with dyes or tracers are needed. The obtained interferograms are evaluated by an intensity analysis of every pixel, resulting in a high lateral resolution of about one micrometre, and the possibility of real-time phase determination. Due to the interferometric nature of the method the phase measurement is unambiguous for optical phase changes in the interval of zero to π radians. We present the expansion of the phase measurement range by a two-wavelength method, allowing us to resolve concentration changes down to 4×10^{-6} mol cm^{-3} and quantify concentrations up to 10^{-3} mol cm^{-3}. The result is an optimization of the resolution by a factor of two and of the dynamic range by a factor of six in comparison to the single-wavelength technique.

Keywords: phase measurement, microfluidics, microscopy, micro-mixing, label-free imaging, interferometry, two-wave mixing, optical image processing

(Some figures in this article are in colour only in the electronic version)

1. Introduction

Micro- and nanofluidic devices are of growing interest in the fields of microscale chemical synthesis and medical diagnostics [1]. The ability to control and manipulate small amounts of fluids (10^{-9}–10^{-18} l) has induced several promising strategies such as micro-total analysis systems (μTAS) [2] or lab-on-a-chip devices (LOC) [3]. One of the most important issues in microfluidics is the mixing of reagents [4]. On the small scales of the microdevices only laminar flows occur and therefore mixing is only based on diffusion and is thus less efficient. To ensure a complete and rapid mixing of reagents, intelligent mixing strategies have to be found. The desired control of quality and temporal behaviour of mixing in newly developed devices requires a non-intrusive, label-free analysis tool with high spatial and temporal resolution. Although fluorescence-based techniques such as laser-induced fluorescence have a great potential according to chemical sensitivity and spatial resolution [5], the dyes used can cause problems due to biotoxic implications [6].

Holographic interferometry is, due to its capability of phase determination, very sensitive for the smallest concentration changes of fluids and at the same time completely non-intrusive. This ability is often used for the measurement of fluidic concentration fields [7–9]. However, one restriction for interferometric concentration measurements is the modulo 2π definition of the phase information, leading to a phase ambiguity for optical path length differences larger than the wavelength. To extend the possible measurement range, typically dual- or multi-wavelength techniques are utilized in holographic and digital holographic interferometry [10–15].

In a previous work, we could show that a photorefractive novelty filter with lithium niobate as the holographic medium

is a promising tool for high sensitivity real-time micro-mixing analysis [16]. This technique transfers temporally changing phase information of an object into intensity information. Thus we call it a *dynamic phase contrast technique*. In this paper, we report on the development of a two-wavelength dynamic phase contrast method in order to increase the measurable phase shift. A further advantage of this technique relies on the independent information out of the two simultaneous phase measurements which leads to a higher accuracy. The application of the two-wavelength dynamic phase contrast technique is demonstrated by analysing concentration changes of a sodium chloride solution in water in a micro-T-mixer and the measurement of the change in the optical path length of a helium jet in air.

2. Dynamic phase contrast

The measurement method is based on real-time holographic interferometry [7, 17] by photorefractive two-beam coupling. Two coherent laser beams are superimposed in a photorefractive material. The resulting interference pattern is translated into a refractive index pattern by the material, and subsequently the beams are diffracted by this index lattice. If the refractive index modulation is shifted with respect to the interference pattern an energy transfer between the two beams occurs. This phase shift can be caused by the photorefractive material itself, as for example in barium titanate [18], or by an externally introduced phase shift [16]. Depending on the coupling strength and diffraction efficiency of the photorefractive material, a complete energy transfer from one beam to the other can be achieved [19]. If the depleted beam is chosen as the signal-bearing beam, the measured intensity of this beam will fall off to zero for a static input signal, and changes in the signal beam, such as variation of amplitude or phase, will instantaneously effect an increased output intensity [20–22]. Therefore this system is often described as a temporal high pass filter, which detects temporally dynamic signals while suppressing the static background (novelty filter) [23]. This behaviour leads to several applications of the method, ranging from bio-compatible dynamic phase contrast microscopy [24] to micro-flow velocity field analysis [25]. Moreover, the output intensity I_{out} is directly dependent on phase variations introduced to the signal beam. Based on theoretical and experimental investigations, the dependence of the dynamic phase contrast output on a phase shift ϕ was found to be described by the following equation [16]:

$$I_{\text{out}} = I_{\max} \sin^2\left(\frac{\phi}{2} + \chi - \frac{\pi}{2}\right), \tag{1}$$

where $I_{\max}$ is the maximum intensity used in the system, which is fixed during the measurement process. The extra phase term χ takes a possible grating phase shift, introduced by the photorefractive material or an external phase shift applied to one of the two beams, into account. For a measurement of phase shifts, the phase transfer function (PTF) of the system has to be determined experimentally by introducing known phase shifts onto either the signal or the reference beam. With this PTF a simple look-up table can be created to determine an unknown phase shift. The simplicity of this dependence allows real-time measurements of phase changes such as those introduced by density changes in fluids [16]. Equation (1) shows that the phase transfer function has a quadratic sinusoidal dependence on the introduced phase shift ϕ. This causes a limited range of uniqueness within the interval from zero to π radians. For measurements of larger phase shifts in realistic liquid and gaseous fluid flows, this limitation has to be eliminated.

3. Two-wavelength dynamic phase contrast

In order to extend the range of uniqueness, at the same time retaining the real-time data acquisition capability, we chose a multiple-wavelength strategy. The optical phase shift ϕ can be written as

$$\phi = \left(\frac{\pi}{\lambda_{\text{i}}}\text{OPD}\right), \tag{2}$$

where OPD is the optical path difference for a phase shift of ϕ and the wavelength λ_{i}. In the case of a constant thickness of the object under investigation this OPD is proportional to the refractive index change of the object. The phase transfer function for different wavelengths can then be written as

$$I_{\text{out,i}} = I_{\max} \sin^2\left(\frac{\pi}{\lambda_{\text{i}}}\text{OPD} + \chi - \frac{\pi}{2}\right). \tag{3}$$

Here $I_{\text{out,i}}$ is the intensity response of the dynamic phase contrast for wavelength λ_{i}. In the following we assume that $\chi = \pi/2$. This assumption is based on the experimental conditions, where we use lithium niobate as the photorefractive material and apply an external phase shift of $\chi = \pi/2$ to the reference beam after the measurement of the phase transfer function.

In the simplest case, two different wavelengths are sufficient for an expansion of the unambiguous phase measurement range. In figure 1(a) the two theoretical phase transfer functions for $\lambda_1 = 532$ nm and $\lambda_2 = 633$ nm are shown. The intensity response of the system to a phase shift can then be described by a tuple of intensity values. The trajectory of this intensity tuple for different phase shift ranges is plotted in figures 1(b)–(d). An unambiguous allocation of an intensity tuple to a phase shift is possible for nearly all phase shifts in a finite value range (figures 1(b) and (c)). The single intersections can be resolved by assuming a continuous phase change in time or space. If the possible value range of phase changes increases, the phase reconstruction is ambiguous (figure 1 (d)). The non-ambiguous range can be calculated by taking the effective wavelength, which is defined as

$$\lambda_{\text{eff}} = \frac{\lambda_1 \lambda_2}{|\lambda_1 - \lambda_2|}. \tag{4}$$

For the two wavelengths $\lambda_1 = 532$ nm and $\lambda_2 = 633$ nm this effective wavelength is $\lambda_{\text{eff}} = 3.33\ \mu$m, resulting in a maximal range of non-ambiguous phase reconstruction for the two-wavelength method of 12π ($@\lambda_1 = 532$ nm). In reality, inaccuracies in the intensity measurement have to be taken into account. The smallest measurable phase difference $\Delta\phi_{\min}$ depends on the intensity detection system and is less

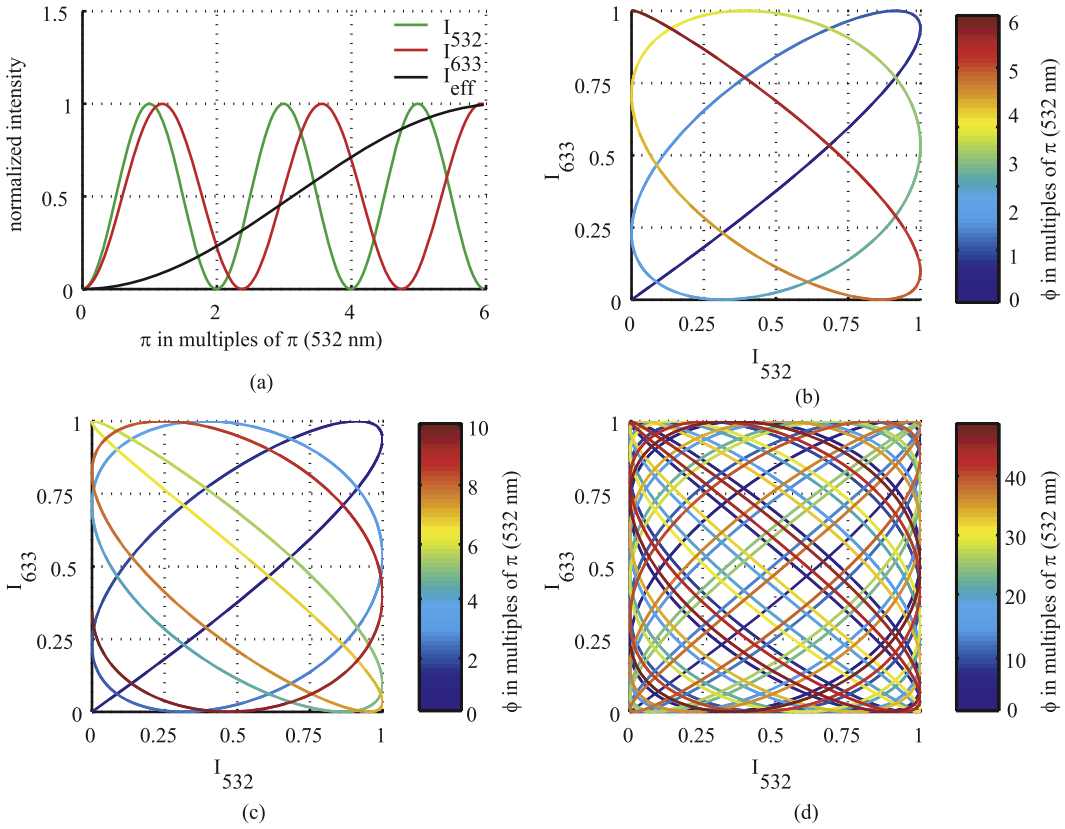

Figure 1. (a) Phase transfer function for two wavelength: 532 and 633 nm. (b)–(c) Trajectory of the tuple of intensity response for different value ranges of phase changes ϕ.

than $\Delta\phi_{\min} = \lambda/20$ or 0.1π at a wavelength of $\lambda_1 = 532$ nm. This decreases the non-ambiguous phase measurement range to a value of about 6π. Nevertheless this is a large extension of the technique compared to the single-wavelength method.

4. Experimental implementation

For the investigation of microfluidic mixing processes we implemented the two-wavelength dynamic phase contrast technique into a microscope set-up as sketched in figure 2. The laser beams of a frequency-doubled Nd:YAG laser and an HeNe laser were split into two beams, the signal and the reference, with the help of a polarizing beamsplitter. The signal beams were collimated to illuminate an object, which was imaged with the help of microscope optics onto two CCD cameras, one for each wavelength. These cameras were synchronized and aligned to each other with sub-pixel accuracy. All four beams, the signal beams and the reference beams, were made to interfere in a photorefractive lithium niobate crystal. We choose lithium niobate because of its large photorefractive grating formation time constant, in order to avoid trail formation, which would be detrimental for reliable phase measurements [16, 22]. The reference beams, after getting reflected off the polarizing beamsplitter, were directed onto a piezo-controlled mirror (PM) after passing through a quarter-waveplate ($\lambda/4$). This mirror served as a phase-shifting element for calibrating the system, i.e. determining the PTF of the system.

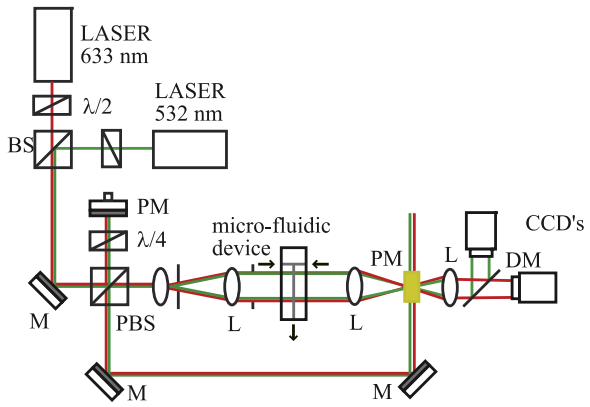

Figure 2. Experimental set-up of the two-wavelength dynamic phase contrast microscope. BS: beamsplitter, CCD: cameras, DM: dichroic mirror, L: lens, M: mirror, PM: photorefractive material, PST: polarizing beamsplitter, $\lambda/2$: half-waveplate, $\lambda/4$: quarter-waveplate.

The measurement of phase changes, introduced by microfluidic processes, was realized in three steps. First the background images, consisting of the microfluidic system with a reference fluid in it, was stored as a hologram in the photorefractive material. Therefore a total laser power of 3 mW for each wavelength was used to store this reference state with an exposure time of 60 s and an intensity beam ratio of approximately one. Subsequently we changed the

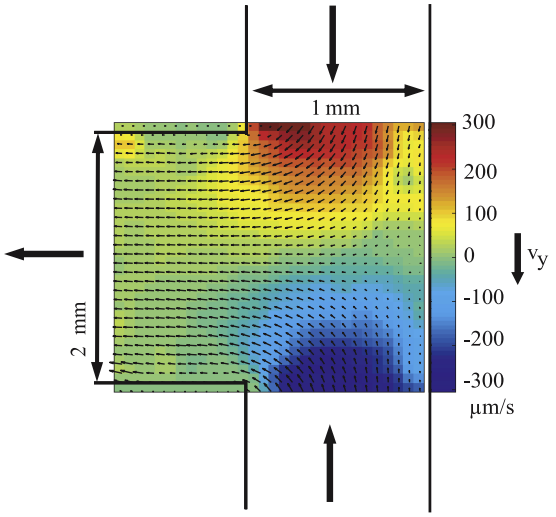

Figure 3. PIV measurement of a typical laminar flow field in the T-channel used for concentration measurements. The y component of velocity is visualized by the colour-coded background.

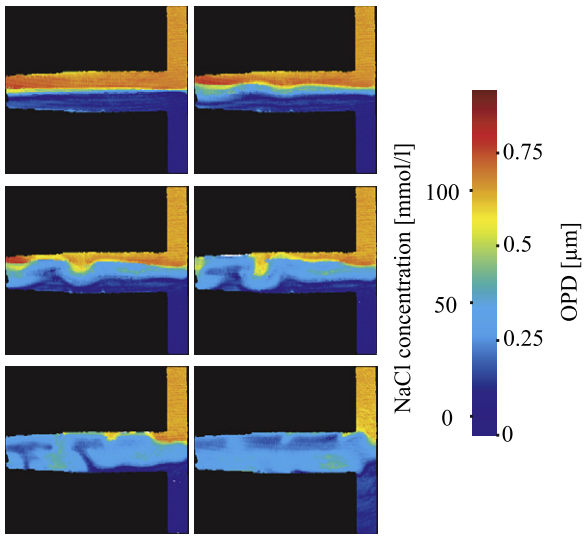

Figure 4. Measurement of concentration changes due to diffusive mixing of an NaCl solution (85.5 mmol l^{-1}) in water. The inflow of the two fluids was stopped after taking the first image. The last image was taken 30 s after the first image. The frame rate of the imaging system was 30 fps in this measurement.

intensity ratio of the beams to 1/10 with a total power of 300 nW and introduced a phase shift to the reference beams to set the working point of the dynamic phase contrast output. Because of the reduced total intensity during the readout process, undisturbed measurements could be performed for more than 2 h. We calibrated the system by determining its PTF at each pixel of the CCD camera, in order to reduce the artefacts arising out of inhomogeneous illumination. As the third step we started the phase change measurement.

It is important that the refractive index change due to a concentration change of the test object is the same for both wavelengths. For the two wavelengths $\lambda_1 = 532$ nm and $\lambda_2 = 633$ nm the dispersion difference of pure water and the maximal sodium chloride concentration of 10^{-3} mol cm^{-3} yields an error in optical path length difference of $\pi/75$ [26]. Further error sources of the phase change determination can be caused by vibrations of the set-up or electronic noise of the camera. In order to quantify this error, we performed long-time stability experiments by measuring given optical path length differences. The deviation of the measured values from the predetermined phase shifts was less than $\pi/20$ in all experiments. Because the dispersion difference leads to a much smaller uncertainty of the OPD determination we neglected this error source in the measurements.

5. Analysis of microfluidic mixing processes

To study micro-mixing of liquids, we constructed a T-shaped mixing channel with a height of 500 μm and a channel width of 1 mm for the input channels and 2 mm for the outflow. After storing the initial holograms of the T-channel with water in it and measuring the PTF, we started the phase change measurement and let an NaCl solution in water (85.5 mmol l^{-1}) flow into the channel. In this experiment the liquids were pumped into the channel with a syringe pump with an average flow rate of 18 mm s^{-1}, resulting in a laminar flow. The 2D velocity field, measured by particle image velocimetry in this T-channel, is shown in figure 3.

Due to the laminar nature of the flow, the two liquids do not mix with each other. A diffusive mixing process was introduced by stopping the flow and was analysed by comparing the output intensities with the PTF. Due to a linear relationship of the refractive index and the concentration C of an aqueous sodium chloride solution for the two wavelengths of $\lambda_1 = 532$ nm and $\lambda_2 = 633$ nm [26] we can calculate the concentration change ΔC from the optical path length difference, OPD:

$$\Delta C = k\Delta n = \frac{k}{d}\mathrm{OPD} = K\,\mathrm{OPD}. \tag{5}$$

The constant factor k is dependent on the fluid, the temperature and the pressure of the fluid. Therefore in the experiment it is more accurate to determine the factor K by measuring the optical path length difference of a standard with known concentrations at the same conditions of temperature and pressure as in the following measurement. Uncertainties because of channel thickness deviations can be suppressed in the same way as illumination inhomogeneities by determining K for every pixel. Figure 4 shows the result after the calibration has been applied to the images. The minimum change in the optical path length that we can currently detect with the system is related to $\lambda/40$, which corresponds to a concentration change of 4×10^{-6} mol cm^{-3} for a channel thickness of 500 μm. The maximal concentration change in the unique reconstruction range is now up to 10^{-3} mol cm^{-3}, which is an increase by a factor of six in comparison to the single-wavelength method.

6. Visualization of gas flows

For a demonstration of the capability to visualize gaseous flows we choose a gas mixing chamber as shown in figure 5. The

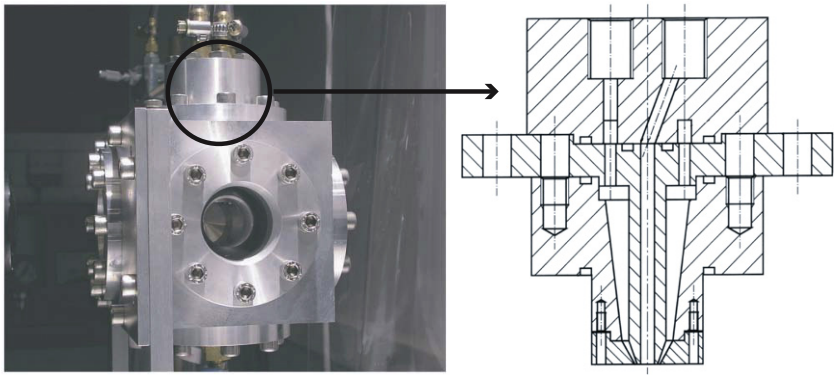

Figure 5. Gas mixing chamber for analysis of gaseous flows. Left: photograph of the chamber. The length of the chamber is 60 mm, while the diameter of the observation windows is 25 mm. Right: sketch of the coaxial nozzle. The diameter of the inner channel is 3 mm, while the diameter of the outer ring channel is 5.4 mm.

temperature and pressure inside this chamber are adjustable to ensure stable measurement conditions. The inlet is realized as a coaxial nozzle as sketched on the right side of figure 5 and can be used to mix two gases. The inner diameter of the nozzle is $d = 3$ mm and the outer diameter is $d = 5.4$ mm. The full width of the chamber in the viewing direction is $l = 60$ mm, while the diameter of the observation windows is 25 mm. The measurement procedure is the same as described in the previous section for liquid flows. As the initial state we stored the holograms of the mixing chamber with air in it. Hereafter we measured the phase transfer function and calibrated the system by introducing known phase shifts by the piezo-mirror. As a first example we choose helium as a test gas and compressed it with $p_{\mathrm{He}} = 2$ bar through the inner channel of the nozzle. The surrounding medium was air at a pressure of $p_{\mathrm{air}} = 1$ bar, resulting in a refractive index difference of about $\Delta n = 2.3 \times 10^{-4}$. Because of the faster velocities in the gaseous flow relative to the liquid flows we changed the camera settings to 70 frames per second and an exposure time of 50 μs. In figure 6 the calibrated results show a phase shift of $\phi = 1.5$ μm or 5.6π(@$\lambda_1 = 532$ nm) introduced by the helium jet. This phase shift is close to the maximal possible phase shift of $\phi_{\mathrm{max}} = 1.66$ μm or 6.2π(@$\lambda_1 = 532$ nm) which can be determined unambiguously by the system. In the case of this fully three-dimensional object it has to be pointed out that the dynamic phase contrast integrates the phase shift over the full length of the mixing chamber. The measurements are projections of the three-dimensional system onto a two-dimensional plane. For a fully three-dimensional determination of phase shifts the dynamic phase contrast can be combined, for example, with tomographic techniques.

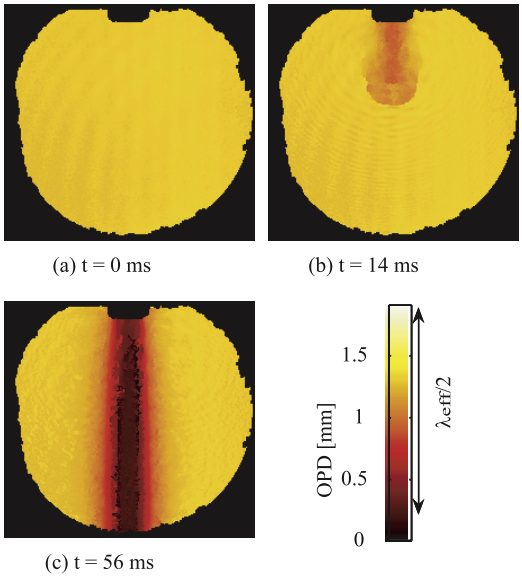

Figure 6. Determination of the phase shift introduced by a helium jet in air. The round aperture in the images is 25 mm in diameter and the nozzle is a coaxial nozzle with a diameter of 3 mm.

7. Conclusion

We have presented a dynamic phase contrast microscopy system based on holographic interferometry. For the extension of the phase measurement range we developed a two-wavelength method and could show an expansion of the measurement range by a factor of six. This development enables us to investigate density changes in liquid systems as well as gaseous flows in real time with high resolution. We studied the mixing process of two liquids, namely a sodium chloride solution in water. The achieved accuracy of the concentration measurement was better than 4×10^{-6} mol cm^{-3}. In a gaseous flow system we could measure the phase shift introduced by a helium jet in air to be 1.5 μm or 5.6π (@532 nm). The contact- and tracer-free nature, the low power requirements and the real-time operability of this technique makes it a promising tool for micro- and macrofluid flow analysis.

Acknowledgments

The authors would like to thank the Deutsche Forschungsgemeinschaft for financial support of this project in the frame of the priority programme SPP 1147 and the Transregional Collaborative Research Centre TRR 61.

References

[1] Whitesides G M 2006 The origins and the future of microfluidics *Nature* **442** 368–73

[2] Manz A, Graber N and Widmer H M 1990 Miniaturized total chemical analysis systems: a novel concept for chemical sensing *Sensors Actuators* B **1** 244–48

[3] Geschke O, Klank H and Tellman P 2004 *Microsystem Engineering of Lab-on-a-Chip Devices* (New York: Wiley)

[4] Sinton D 2004 Microscale flow visualization *Microfluid. Nanofluid.* **1** 2–21

[5] Dittrich P S and Manz A 2005 Single-molecule fluorescence detection in microfluidic channels–the Holy Grail in muTAS? *Anal. Bioanal. Chem.* **382** 1771–82

[6] Parak W J, Pellegrino T and Plank C 2005 Labelling of cells with quantum dots *Nanotechnology* **16** R9–25

[7] Vest C M 1979 *Holographic Interferometry* (New York: Wiley)

[8] Watt D W and Vest C M 1987 Digital interferometry for flow visualization *Exp. Fluids* **5** 401–6

[9] Yuan B, Chen S, Yang X, Wang C and Li L 2008 Mapping the transient concentration field within the diffusion layer by use of the digital holographic reconstruction *Electrochem. Commun.* **10** 392–6

[10] Polhemus C 1973 Two-wavelength interferometry *Appl. Opt.* **12** 2071–4

[11] Wagner C, Osten W and Seebacher S 2000 Direct shape measurement by digital wavefront reconstruction and multiwavelength contouring *Opt. Eng.* **39** 279–85

[12] Wada A, Kato M and Ishii Y 2008 Multiple-wavelength digital holographic interferometry using tunable laser diodes *Appl. Opt.* **47** 2053–60

[13] Mann C J, Bingham P R, Paquit V C and Tobin K W 2008 Quantitative phase imaging by three-wavelength digital holography *Opt. Express* **16** 9753–64

[14] Kühn J, Colomb T, Montfort F, Charrire F, Emery Y, Cuche E, Marquet P and Depeursinge C 2007 Real-time dual-wavelength digital holographic microscopy with a single hologram acquisition *Opt. Express* **15** 7231–42

[15] Parshall D and Kim M 2006 Digital holographic microscopy with dual wavelength phase unwrapping *Appl. Opt.* **45** 451–9

[16] Krishnamachari V V, Grothe O, Deitmar H and Denz C 2005 Novelty filtering with a photorefractive lithium–niobate crystal *Appl. Phys. Lett.* **87** 071105

[17] Hariharan P 1996 *Optical Holography: Principles, Techniques and Applications* (Cambridge: Cambridge University Press)

[18] Feinberg J, Heiman D, Tanguay A R and Hellwarth R W 1980 Photorefractive effects and light-induced charge migration in $BaTiO_3$ *J. Appl. Phys.* **51** 1297–305
Feinberg J, Heiman D, Tanguay A R and Hellwarth R W 1980 *J. Appl. Phys.* **51** 1297

[19] Kukhtarev N V, Markov V B, Odulov S G, Soskin M S and Vinetskii V L 1979 Holographic storage in electro-optic crystals 2: beam-coupling light amplification *Ferroelectrics* **22** 961–4

[20] Sedlatschek M, Rauch T, Denz C and Tschudi T 1995 Demonstrator concepts and performance of a photorefractive optical novelty filter *Opt. Mater.* **4** 376–80

[21] Sedlatschek M, Trumpfheller J, Hartmann J, Müller M, Denz C and Tschudi T 1999 Differentiation and subtraction of amplitude and phase images using a photorefractive novelty filter *Appl. Phys.* B **68** 1047–54

[22] Krishnamachari V V and Denz C 2003 Real-time phase measurement with a photorefractive novelty filter microscope *J. Opt.* A **5** 239–40

[23] Anderson D Z and Feinberg J 1989 Optical novelty filters *IEEE J. Quantum Electron.* **25** 635–47

[24] Petermeier H, Kowalczyk W, Delgado A, Denz C and Holtmann F 2007 Detection of microorganismic flows by linear and nonlinear optical methods and automatic correction of erroneous images artefacts and moving boundaries in image generating methods by a neuronumerical hybrid implementing the Taylor's hypothesis as *a priori* knowledge *Exp. Fluids* **42** 611–23

[25] Woerdemann M, Holtmann F and Denz C 2008 Full-field particle velocimetry with a photorefractive optical novelty filter *Appl. Phys. Lett.* **93** 021108

[26] Washburn E W 2003 *International Critical Tables of Numerical Data, Physics, Chemistry and Technology* (New York: Knovel)